1 Principles of Comparative Crystal Chemistry[1]

Robert M. Hazen*, Robert T. Downs‡ and Charles T. Prewitt*

**Geophysical Laboratory and Center for High-Pressure Research*
Carnegie Institution of Washington
5251 Broad Branch Road NW,
Washington, DC 20015

and

‡Department of Geosciences
University of Arizona
Tucson, Arizona 85721

INTRODUCTION

The art and science of crystal chemistry lies in the interpretation of three-dimensional electron and nuclear density data from diffraction experiments in terms of interatomic bonding and forces. With the exception of meticulous high-resolution studies (e.g. Downs 1983, Downs et al. 1985, Zuo et al. 1999), these density data reveal little more than the possible atomic species and their distributions within the unit cell. Other parameterizations of crystal structures, including atomic radii, bond distances, packing indices, polyhedral representations, and distortion indices, are model-dependent. These secondary parameters have proven essential to understanding structural systematics, but they are all based on interpretations of the primary diffraction data.

Comparative crystal chemistry carries this interpretive process one step further, by comparing parameters of a given structure at two or more sets of conditions. In this volume we focus on structural variations with temperature or pressure, though the general principles presented here are just as easily applied to structural variations with other intensive variables, such as electromagnetic field, anisotropic stress, or composition along a continuous solid solution. Two or more topologically identical structures at different temperatures or pressures may vary slightly in unit-cell parameters and atomic positions, thus adding a variable of state to the structural analysis.

A straightforward procedure for reporting structural data at a sequence of temperatures or pressures is to tabulate the standard primary parameters (unit-cell parameters, fractional atomic coordinates and thermal vibration coefficients, along with refinement conditions) and secondary parameters (e.g. individual and mean cation-anion bond distances, bond angles, polyhedral volumes and distortion indices) for each set of conditions. Most such structural studies also include graphical illustrations of the variation of key secondary parameters with temperature or pressure. In addition, several useful comparative parameters, including bond compressibilities and thermal expansivities, polyhedral bulk moduli, and strain ellipsoids, have been devised to elucidate structural variations with temperature or pressure, and to facilitate comparisons of this behavior among disparate structures.

The principal objective of this chapter is to define the most commonly cited comparative parameters and to review some general trends and principles that have emerged from studies of structural variations with temperature and pressure.

---

[1] This chapter is adapted, in part, from *Comparative Crystal Chemistry* (Hazen and Finger 1982).

1529-6466/00/0041-0001$05.00

THE PARAMETERS OF A CRYSTAL STRUCTURE

A complete description of the structure of a crystal requires knowledge of the spatial and temporal distributions of all atoms in the crystal. By definition the crystal has periodicity, so the spatial terms can be represented by (1) the size and shape of the unit cell, (2) the space group, and (3) the fractional coordinates of all symmetrically distinct atoms along with their associated elemental compositions. A complete description of the temporal variation is impossible for all real materials and a simplifying assumption of independent atoms with harmonic vibrations is usually made. This assumption implies thermal ellipsoids of constant probability density, which constitute the fourth element of the structure description (see Downs, this volume, for a discussion of thermal motion and its analysis). The determination of these structural parameters remains a major objective of crystallographers.

Although the majority of structures can be characterized by these four elements alone, many atomic arrangements are more easily conceptualized with the aid of additional descriptors derived from the basic set. Many crystal structures, especially those of mineral-like phases, are traditionally described in terms of nearest-neighbor clusters of atoms. Most structural parameters, including cation-anion bond distances, interatomic angles (both anion-cation-anion and cation-anion-cation), polyhedral volumes and polyhedral distortion indices, thus relate to cation coordination polyhedra. These parameters are reviewed briefly below.

Interatomic distances

Equilibrium distances between pairs of bonded atoms represent the most important single factor in determining a compound's crystal structure (Pauling 1960). The bonding environment for a given pair of ions is similar over a wide range of structures, and thus enables an analysis of structures by isolating nearest-neighbor clusters (e.g. Gibbs 1982). Boisen and Gibbs (1990) present a straightforward matrix algebra approach to the calculation of bond distances between two atoms at fractional coordinates (x_1,y_1,z_1) and (x_2,y_2,z_2) for a crystal with unit-cell parameters a, b, c, α, β, and γ. This value is the distance most commonly reported in crystallographic studies. A program for calculating bond distances and angles, known as METRIC, is incorporated into the XTALDRAW software written by Downs, Bartelmehs and Sinnaswamy, and is available on the Mineralogical Society of America website. The METRIC software was written by Boisen, Gibbs, Downs and Bartelmehs.

Thermal corrections to bond distances. An important and often neglected aspect of bond distance analysis is the effect of thermal vibrations on mean interatomic separation. Busing and Levy (1964) noted that "the atomic coordinates resulting from a crystal structure analysis represent the maximum or the centroid of a distribution of scattering density arising from the combined effects of atomic structure and thermal displacement." Interatomic distances reported in most studies are calculated as the distance between these atomic positions. However, as Busing and Levy demonstrate, a better measure of interatomic distance is the *mean* separation. In general, the mean separation of two atoms will always be greater than the separation between the atomic positions as determined by refinement under the independent atom assumption. Thus, thermal expansion based on a mean separation may be greater, and may represent a more valid physical interpretation, than that reported in most recent studies.

Calculation of precise mean separation values requires a detailed understanding of the correlation of thermal motions between the two atoms. While this information is not available for most materials, it is possible to calculate lower and upper limits for mean interatomic distances. In addition, the special cases of riding motion and non-correlated vibrations may be calculated using equations cited by Busing and Levy (1964). Lower bound, upper bound, riding, and non-correlated thermally corrected bond distances are computed by the least-squares refinement program RFINE (Finger and Prince 1975).

One possible correlated motion is the rigid-body motion that is exhibited by the atoms in a molecule that are tightly bonded to each other (Shomaker and Trueblood 1968). The SiO_4 group offers a good example (Bartelmehs et al. 1995). The Si and O atoms vibrate as a group, as if held together by rigid rods, between the Si and O atoms and also between the four O atoms. The mathematics for recognizing and treating the rigid-body case is carefully laid out in a chapter by Downs (this volume). Downs et al. (1992) determined a simple equation for computing the bond length correction between a cation and an anion that are held with a strong rigid bond, but not necessarily part of a rigid body,

$$R^2_{SRB} = R^2 + \frac{3}{8\pi^2}[B_{iso}(A) - B_{iso}(C)]$$

where R_{SRB} is the length of the simple rigid bond, R is the observed bond length, and $B_{iso}(A)$ and $B_{iso}(C)$ are the isotropic temperature factors for the anions and cation, respectively. This equation produces a corrected bond length that generally agrees with the rigid body model to within 0.001 Å and is suitable for application to many tetrahedral and octahedral bonds found in minerals. A systematic study of the correction to bond lengths and volumes of SiO_4 groups determined as a function of temperature can be found in Downs et al. (1992).

It is important to understand the physical significance of the various types of thermally corrected interatomic distances, which are summarized below.

1. *Lower Bound Corrections*: The lower bound of mean separation may result from highly correlated parallel motions of the two atoms. This distance will closely approximate the uncorrected centroid separation, because atoms vibrating in parallel have nearly constant separation equal to that of the atomic coordinate distance.
2. *Upper Bound Corrections*: The upper bound of mean separation occurs if atoms vibrate in highly correlated anti-parallel motion. For instance, if one atom is vibrating perpendicular to the bond in an upwards direction, then the other is vibrating downwards.
3. *Riding Corrections*: Riding corrections are applicable to the case where one lightweight atom's vibrations are superimposed on the vibrations of another, heavier atom, as in the case of a hydrogen bonded to an oxygen atom. Riding corrections are usually only slightly larger than lower bound corrections, because both involve parallel and correlated motions.
4. *Non-correlated Corrections*: Non-correlated motions, as the name implies, are represented by atoms that do not directly interact, as in non-bonded atoms of molecular crystals. Such corrections, which are clearly intermediate between those of correlated parallel and anti-parallel motions, might be applicable to cation-cation distances in some silicates. Furthermore, if cation-anion distances in silicates are presumed to have more parallel than anti-parallel motion, then the non-correlated distance may serve as the upper limit for thermally corrected cation-anion bond distances.
5. *Rigid Body Motion*: Rigid body motion is applicable if a group of atoms vibrate in tandem, with identical translational component and an oscillatory librational

component. The model was developed for molecular crystals, but has found application to the strongly bonded polyhedral units found in many Earth materials. The magnitude of correction is similar to that provided by the riding correction but applicable to heavier atom such as in SiO_4, or MgO_6.

In their careful study of the effect of temperature on the albite structure, Winter et al. (1977) demonstrate the Busing and Levy (1964) corrections on various Al-O, Si-O and Na-O bonds. We modify their figure showing the variation in the Al-OA1 bond lengths versus temperature to include the rigid body correction (Fig. 1). The magnitude of thermal corrections, naturally, depends upon thermal vibration amplitudes. Thus, at high temperatures thermal corrections can be as large as 5% of the uncorrected distance.

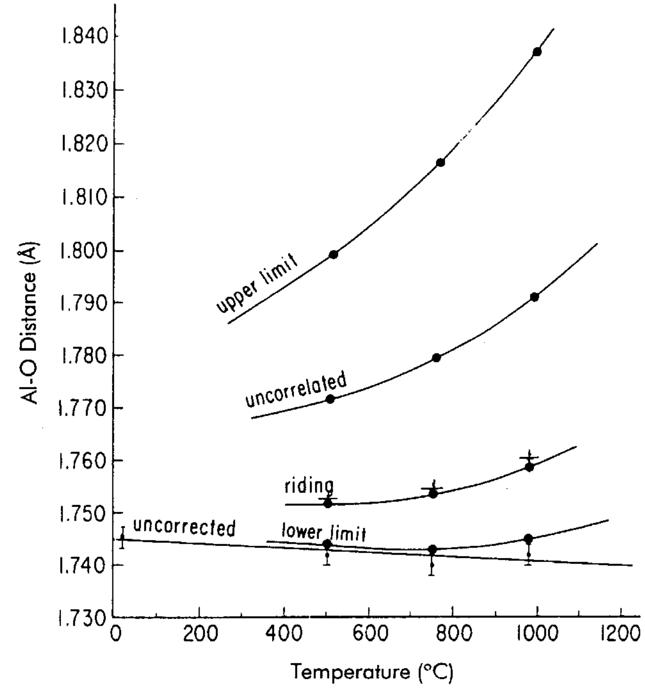

Figure 1. A plot of the length of the Al-OA1 bond versus temperature for low albite, modified from Winter et al. (1977). The bond length is corrected for the Busing and Levy (1964) effects, as indicated by solid lines, as well as for rigid body motion, as indicated by the cross-marks located just above the riding correction.

Ionic radi. Expected cation-anion bond distances at ambient conditions may be systematized by developing tables of internally-consistent ionic radii—an approach pioneered by the work of Bragg, Lande, Goldschmidt and others (see Pauling 1960). One of the most widely quoted radii tables was developed by Shannon and Prewitt (1970) and revised by Shannon (1976). All radii tables require the assumption of one standard radius, because diffraction experiments provide information on interatomic distances. Shannon and Prewitt set the radius of oxygen at 1.40 Å, in accord with the value chosen by Pauling.

A consequence of the 1.40 Å value for oxygen is that anions are modeled as larger than cations in most mineral-like compounds. Not all authors agree with this concept of "small" cations, however. Slater (1963) and Prewitt (1977) have suggested that smaller anions may be more realistic. O'Keeffe and Hyde (1981) have proposed, alternatively, that two sets of radii should be considered in the description of structure. Bonded radii are similar to the Pauling and the Shannon and Prewitt sizes, with anions larger than cations. In addition, O'Keeffe and Hyde propose the use of "nonbonded" radii for next-nearest neighbor anions. In this formulation, the nonbonded radii for cations are significantly greater than for anions. These second-nearest neighbor radii have been used successfully to explain the near constant distance of some cation-cation pairs, such as Si-Si, in a wide variety of structures.

Gibbs and co-workers (cf. Gibbs et al. 1992) have argued that the various sets of radii should only be used to generate bond lengths and are not to be confused with indicating the physical size of atoms in crystals. Electron density maps can provide information on the physical size of atoms, determined from the location of minima in the density along the bonds. Such an approach shows that there is no single radius for a given atom, but that it varies from bond to bond. In general, however, these maps demonstrate that the size of the O atom is more-or-less similar to the radius provided by the Shannon (1976) model. The large cation radii of the O'Keefe and Hyde (1981) model are consistent with the diffuse electron density of cations.

Interbond angles

Interbond or interatomic angles are secondary parameters of a crystal structure that quantify the angle in space defined by three adjacent atoms. Boisen and Gibbs (1990) present a matrix algebra formulation for the general case of calculating a bond angle $\theta_{1\text{-}2\text{-}3}$ that is defined by a central atom at fractional coordinates (x_1,y_1,z_1) and two other atoms at (x_2,y_2,z_2) and (x_3,y_3,z_3), for a crystal with unit-cell parameters a, b, c, α, β, and γ. The XTALDRAW software provides bond angle calculations based on this scheme.

Two types of interbond angles are most commonly reported. Nearest-neighbor cation-anion-cation angles are often tabulated when the two cations are situated in coordination polyhedra that share corners. Thus, Si-O-Si angles are invariably cited in descriptions of chain silicates (see Yang and Prewitt, this volume), and Si-O-Al angles are reported for framework aluminosilicates (see Ross, this volume). In addition, intrapolyhedral anion-cation-anion angles are commonly listed for cations in 2-, 3-, 4-, 5- or 6-coordination. Note that in the case of 5- and 6-coordinated cations a distinction can be made between adjacent and opposite anion-cation-bonds. In a regular cation octahedron, for example, adjacent anion-cation-anion bond angles are 90°, whereas opposite bond angles are 180°.

Bond angles have always been calculated on the basis of centroid atom positions, without regard to thermal motion. This convention, however, may result in misleading values of bond angles in special cases, most notably in the situation of Si-O-Si bonds that are constrained by symmetry to be 180° (e.g. in thortveitite $ScSi_2O_7$ and high cristobalite SiO_2). In these cases, the spatially averaged bond angle is always significantly less than 180°, because thermal motion of the oxygen atom is toroidal. Thus, the oxygen atom rarely occupies a position midway between the two silicon atoms. Nevertheless, the time-averaged oxygen position is constrained to lie on a straight line between the silicon atoms, so the calculated angle is 180°. In the case of a rigid polyhedron, it is possible to compute thermally corrected angles from an analysis of the rigid body motion, as described in the chapter by Downs. The O-Si-O angles in a variety of SiO_4 groups characterized at high temperature (Downs et al. 1992) were found to be quite similar to their uncorrected values. However, corrected bond lengths and ∠Si-O-Si for the silica polymorphs can vary considerably. For instance, R(SiO) = 1.5515 Å and ∠Si-O-Si = 180° for β-cristobalite at 310°C (Peacor 1973). Corrected for SiO_4 rigid body vibration we find that the corrected R(SiO) = 1.611 Å, and a thermally corrected ∠Si-O-Si = 148.8°. This result is in good agreement with room temperature values of 1.607 Å and 146.6°, respectively.

Coordination polyhedra

In numerous compounds, including most of those characterized as "ionic" by Pauling (1960), it is useful to examine cation coordination polyhedra as subunits of the structure. Their volumes and their deviations from ideal geometrical forms, furthermore, may provide useful characterizations of these subunits.

Polyhedral volumes. In most cases of cations coordinated to four or more nearest-neighbor anions, the coordination polyhedron may be treated as a volume that is defined as the space enclosed by passing planes through each set of three coordinating anions. Software to calculate polyhedral volumes is available from http://www.ccp14.ac.uk/. One such computer program is described by Swanson and Peterson (1980).

Polyhedral distortions. Cation coordination polyhedra in most ionic structures only approximate to regular geometrical forms. Deviation from regularity may be characterized, in part, by using distortion parameters. Two commonly reported polyhedral distortion indices are quadratic elongation and bond angle variance, which are based on values of bond distances and bond angles, respectively (Robinson et al. 1971).

Quadratic elongation, $\langle\lambda\rangle$, is defined as:

$$\langle\lambda\rangle = \sum_{i=1}^{n} [(l_i/l_0)^2/n] \qquad (1)$$

where l_0 is the center-to-vertex distance of a regular polyhedron of the same volume, l_i is the distance from the central atom to the ith coordinating atom, and n is the coordination number of the central atom. A regular polyhedron has a quadratic elongation of 1, whereas distorted polyhedra have values greater than 1.

Bond angle variance, σ^2, is defined as:

$$\sigma^2 = \sum_{i=1}^{n} [(\theta_i - \theta_0)^2/(n-1)] \qquad (2)$$

where θ_0 is the ideal bond angle for a regular polyhedron (e.g. 90° for an octahedron or 109.47° for a tetrahedron), θ_i is the ith bond angle, and n is the coordination number of the central atom. Angle variance is zero for a regular polyhedron and positive for a distorted polyhedron. Robinson et al. (1971) showed that $\langle\lambda\rangle$ and σ^2 are linearly correlated for many silicates and isomorphic structures. However, Fleet (1976) showed that this correlation is not mandated by theory and does not hold true for all structure types.

Quadratic elongations and bond angle variances are scalar quantities so they provide no information about the geometry of polyhedral distortions. For example, it may be possible that an elongated octahedron, a flattened octahedron, or an octahedron with all different bond distances all have the same quadratic elongation ($\langle\lambda\rangle > 1$) and bond angle variance. Similarly, one can imagine a wide range of distorted shapes for octahedra with six identical cation-anion bond distances (quadratic elongation, $\langle\lambda\rangle \approx 1$), but significant angular distortions. For this reason it is often useful to illustrate distorted polyhedra with ball-and-stick drawings that include distance and angle labels.

Standard computer programs for calculating polyhedral volumes also usually provide calculations of quadratic elongation and bond angle variance, along with their associated errors, for octahedra and tetrahedra. The XTALDRAW software provides calculations of these sorts of parameters.

An alternative parameterization of polyhedral distortions was proposed by Dollase (1974), who developed a matrix algebra approach. He describes distortions in terms of a "dilational matrix," which compares the observed polyhedron with an idealized polyhedron. This approach permits the calculation of the degree of distortion relative to an idealized polyhedron of lower than cubic symmetry (i.e. how closely might the observed polyhedron conform to tetragonal or trigonal symmetry). In spite of the rigor of this approach, especially compared to scalar quantities of quadratic elongation and bond angle variance, the Dollase formulation has not been widely adopted.

COMPARATIVE PARAMETERS

Closely related structures, such as two or more members of a solid solution series or the structure of a specific compound at two or more different temperatures or pressures, may be described with a number of *comparative* parameters (hence the title of this chapter, "...*Comparative Crystal Chemistry*"). Comparative parameters add no new data to descriptions of individual crystal structures, but they are invaluable in characterizing subtle changes in structure. The reader should be aware that many of these comparisons involve subtraction, explicit or implicit, of two quantities of similar magnitude. In such cases the error associated with the difference may become very large. It is essential to propagate errors in the initial parameters to the derived quantity being investigated. For example, if $y = x_1 - x_2$, then $\sigma^2_y = \sigma^2_{x1} + \sigma^2_{x2}$. See also, for example, Hazen and Finger (1982).

Changes in unit-cell parameters: the strain ellipsoid

Unit-cell parameters vary systematically with temperature and pressure, and a number of approaches have been developed to parameterize these changes. The most fundamental unit-cell change relates to volume compression and thermal expansion, as considered in the chapter on equations of state (see Angel, this volume). In addition, one can consider axial changes (linear thermal expansion and compression) and the strain ellipsoid, which quantifies the change in shape of a volume element between two sets of conditions.

Linear changes of the unit cell are relatively easy to measure and they provide important information regarding structural changes with temperature or pressure. As uniform temperature or hydrostatic pressure is applied to a crystal, a spherical volume element of the original crystal will, in general, deform to an ellipsoid. Symmetry constraints dictate that this ellipsoid must have a spherical shape in cubic crystals. In uniaxial (trigonal, hexagonal and tetragonal) crystals this strain ellipsoid must also be uniaxial and be aligned with the unique crystallographic axis. In orthorhombic crystals the principal axes of the strain ellipsoid must be aligned with the orthogonal crystallographic axes. Therefore, axial changes of the unit-cell completely define the dimensional variation of the lattice and the strain ellipsoid in the cubic, hexagonal, trigonal, tetragonal and orthorhombic cases.

In each of the cases noted above, the strain ellipsoid's maximum and minimum directions of compression or expansion are parallel to the crystallographic axes and can be calculated directly from unit-cell parameters. A useful parameter in these instances is the anisotropy of compression or thermal expansion, which is given by the length change of the strain ellipsoid's major axis divided by the length change of the ellipsoid's minor axis.

In monoclinic and triclinic crystals, on the other hand, unit-cell angles may also vary. A cataloging of changes in each axial direction does not, therefore, reveal all significant changes to the unit cell. In the triaxial strain ellipsoid, major and minor ellipsoid axes represent the orthogonal directions of maximum and minimum change in the crystal. Relationships between the strain ellipsoid and the crystal can be calculated as described by Ohashi and Burnham (1973).

The usefulness of the strain ellipsoid is illustrated by considering the behavior of albite ($NaAlSi_3O_8$) at high temperature. All three crystallographic axes of this triclinic mineral are observed to expand between room temperature and 900°C. Calculation of the strain ellipsoid, however, reveals that one principal direction actually contracts as temperature is increased (Ohashi and Finger 1973).

The strain ellipsoid may be derived from two related sets of unit-cell parameters as follows (modified after Ohashi and Burnham 1973). Let $\mathbf{a}_i$, $\mathbf{b}_i$, $\mathbf{c}_i$ represent direct unit-cell vectors before ($i = 0$) and after ($i = 1$) a lattice deformation. A strain tensor [**S**] may be defined in terms of these vectors, such that:

$$\mathbf{S} \cdot \mathbf{a}_0 = \mathbf{a}_1 - \mathbf{a}_0 \qquad (3)$$

In matrix notation, define the bases $D_0 = \{a_0, b_0, c_0, \alpha_0, \beta_0, \gamma_0\}$ and $D_1 = \{a_1, b_1, c_1, \alpha_1, \beta_1, \gamma_1\}$. Also define A_0 and A_1 to be matrices that transform from the direct-space systems of D_0 and D_1 to a Cartesian system such that $A_0[v]_0 = [v]_C$ and $A_1[v]_1 = [v]_C$. These transformation matrices can be constructed in an infinite number of ways, but a popular choice is Equation (2.31) in Boisen and Gibbs (1990),

$$A = \left[[a]_C \middle| [b]_C \middle| [c]_C\right] = \begin{bmatrix} a\sin\beta & -b\sin\alpha\cos\gamma^* & 0 \\ 0 & b\sin\alpha\sin\gamma^* & 0 \\ a\cos\beta & b\cos\alpha & c \end{bmatrix} \qquad (4)$$

Equation (3) can then be rewritten as

$$S \cdot A_0 = A_1 - A_0,$$

where A_0 and A_1 are obtained from Equation (4) using the appropriate cell parameters. The strain matrix can be computed by

$$S = S\,A_0A_0^{-1} = A_1A_0^{-1} - A_0A_0^{-1} = A_1A_0^{-1} - I_3.$$

The resulting strain matrix may not represent an ellipsoid because it may not be symmetric, so most researchers transform it into the symmetric strain tensor, ε, which is defined as

$$\varepsilon = [S + S^t]/2 \qquad (5)$$

In general, *unit strain* results are reported. These are defined as the fractional change of major, minor and orthogonal intermediate strain axes per K or per GPa, combined with the angles between strain axes and crystallographic axes. Software (Ohashi 1982) to calculate the strain ellipsoids from unit-cell data is provided at the Mineralogical Society of America website, http://www.minsocam.org.

Changes in bond distances: thermal expansion

The addition of heat to an ionic crystal increases the energy of the crystal, primarily in the form of lattice vibrations or phonons, manifest in the oscillation of ions or groups of ions. When ionic bonds are treated as classical harmonic oscillators, the principal calculated effect of temperature is simply increased vibration amplitude, with eventual breakage of bonds at high temperature as a result of extreme amplitudes. This model is useful in rationalizing such high-temperature phenomena as melting, site disordering, or increased electrical conductivity. The purely harmonic model of atomic vibrations is not adequate to explain many properties of crystals, however, and anharmonic vibration terms must be considered in any analysis of the effect of temperature on crystal structure. For instance, the equilibrium bond length remains unchanged in the harmonic model. Programs that incorporate anharmonic treatments of the thermal motion include ANHARM (hans.boysen@lrz.uni-muenchen.de) and Prometheus (kuhs@silly.uni-mki.gwdg.de).

Thermal expansion coefficients. An important consequence of anharmonic motion is thermal expansion, which includes the change in equilibrium bond distance with temperature. Dimensional changes of a crystal structure with temperature may be defined by the coefficient of thermal expansion, α, defined as:

$$\text{Linear } \alpha_l = \frac{1}{d}\left(\frac{\partial d}{\partial T}\right)_P \tag{6}$$

$$\text{Volume } \alpha_V = \frac{1}{V}\left(\frac{\partial V}{\partial T}\right)_P \tag{7}$$

where subscript P denotes partials at constant pressure. Another useful measure is the mean coefficient of expansion between two temperatures, T_1 and T_2:

$$\text{Mean } \alpha(T_1,T_2) = \frac{2}{d_1 + d_2}\left[\frac{(\mathrm{d}_2 - \mathrm{d}_1)}{(\mathrm{T}_2 - \mathrm{T}_1)}\right] \approx \alpha_{\frac{(\mathrm{T1-T2})}{2}} \tag{8}$$

The mean coefficient of thermal expansion is the most commonly reported parameter in experimental studies of structure variation with temperature.

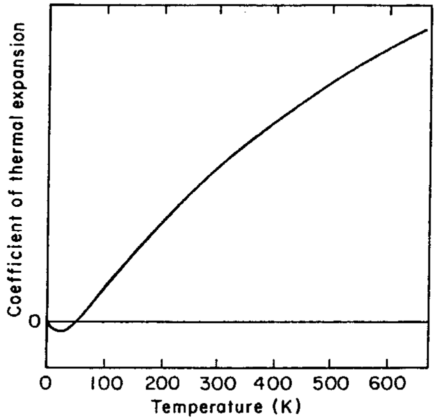

Figure 2. An idealized plot of the coefficient of thermal expansion as a function of temperature for a cation-anion bond or a volume element of an ionic solid. A small range of negative thermal expansion is often observed near absolute zero (after White 1973).

No simple functional form successfully models linear or volume thermal expansion in all materials. The coefficient of thermal expansion is a function of temperature, as illustrated in Figure 2. Near absolute zero, where there is virtually no change in potential energy of a system with temperature, there is also little thermal expansion. In fact, a small range of negative thermal expansion is often observed in compounds below 30 K. As the potential energy increases, so does thermal expansion. For want of a more satisfactory theoretically based equation, most thermal expansion data are presented as a simple second-order polynomial (e.g. Fei 1995):

$$\alpha(T) = a_0 + a_1 T + a_2 T^2 \tag{9}$$

where a_0, a_1, and a_2 are constants determined by fitting the experimental temperature-distance or temperature-volume data.

Systematics of bond thermal expansion. The thermal expansion of a cation-anion bond is primarily a consequence of its interatomic potential. It is not surprising to observe, therefore, that a given type of cation-anion bond displays similar thermal expansion behavior in different structures. Figure 3, for example, illustrates the similar thermal expansion behavior of octahedral Mg-O bonds in a wide variety of oxide and silicate structures. The mean Mg-O bond distance for each symmetrically independent MgO_6 octahedron in these compounds displays near linear thermal expansion between room temperature and the maximum temperatures studied (from 700 to 1000°C), with a coefficient of expansion ~14 (±2) × 10^{-6} K^{-1}. Another example (Fig. 4) is provided by the

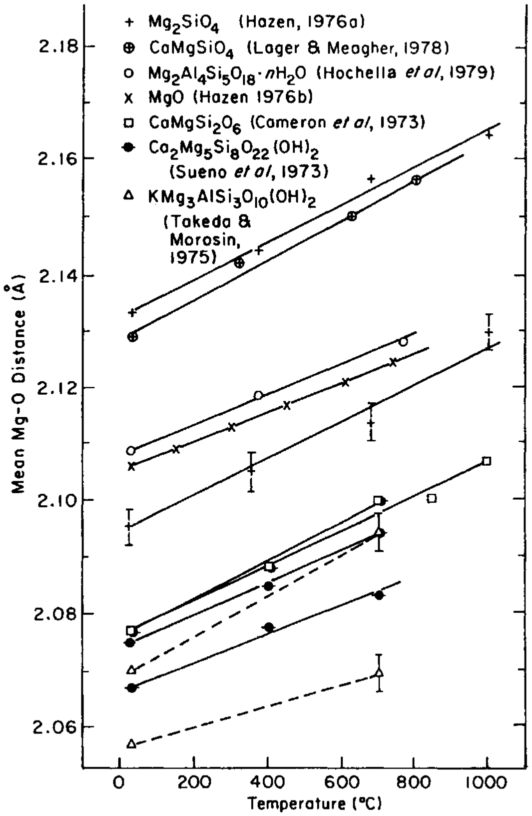

Figure 3. Mean thermal expansion of Mg-O bonds in MgO_6 octahedra is similar in a variety of oxides and silicates (after Hazen and Finger 1982).

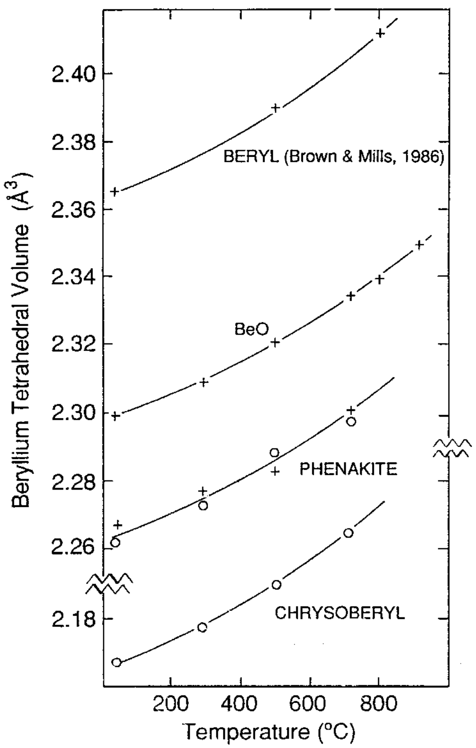

Figure 4. The polyhedral volumes of BeO_4 tetrahedra versus temperature is similar in beryl, bromellite, chrysoberyl and phenakite. Data on BeO are from Hazen and Finger (1986). Be tetrahedral expansions in all four structures display similar curvature (after Hazen and Finger 1987).

thermal expansion of BeO_4 tetrahedra in the oxide bromellite (BeO), in the ring silicate beryl ($Be_3Al_2Si_6O_{18}$), in the orthosilicate phenakite (Be_2SiO_4), and in chrysoberyl ($BeAl_2O_4$ with the olivine structure). Tetrahedra in these structures display similar slopes and curvatures in plots of temperature versus bond distance and temperature versus volume.

In spite of the striking similarities in thermal expansion behavior for the average distance of a given type of bond in different structures, significant differences in expansivity are often observed for individual bonds. In the case of forsterite (Mg_2SiO_4 in the olivine structure), for example, the mean expansion coefficient of Mg-O bonds in the M1 and M2 octahedra are both 16 × 10^{-6} K^{-1} (Hazen 1976a). Expansion coefficients for individual Mg-O bonds within these distorted octahedra, however, range from 8 to 30 × 10^{-6} K^{-1}, with longer bonds displaying greater expansion coefficients (Fig. 5). Such thermal expansion anisotropies, which must be analyzed by comparing the behavior of all symmetrically independent cation-anion bonds, are critical to developing insight regarding effects of temperature on crystal structure.

Systematic trends are also revealed

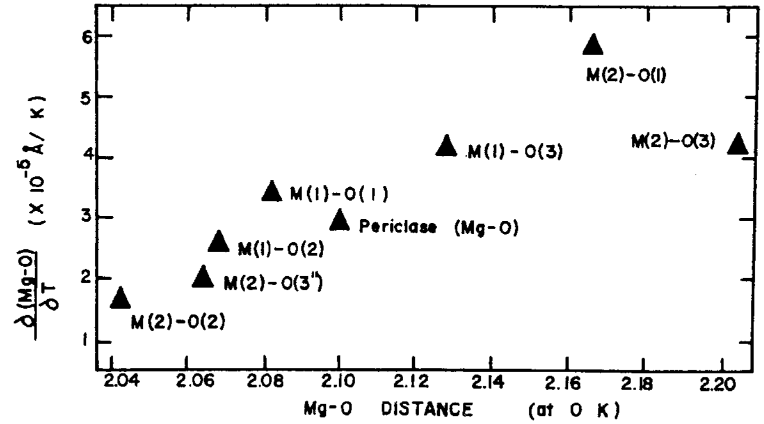

Figure 5. Thermal expansion coefficients of individual Mg-O bonds versus bond distance in forsterite (from Hazen 1976).

by comparison of the magnitude of thermal expansion for different cation-anion bonds. Several previous workers have noted that thermal expansion of cation-anion bond distance is most dependent on the Pauling bond strength: the product of formal cation and anion valences, z_c and z_a, divided by coordination number, n. Thermal expansion is largely independent of ionic mass or cation-anion distance. Based on these empirical observations, Hazen and Finger (1982) give a general relation for linear thermal expansion of mean bond lengths:

$$\alpha_{1000} = 4.0(4)\left[\frac{n}{S^2 z_c z_a}\right] \times 10^{-6}\,\mathrm{K}^{-1} \tag{10}$$

where S^2 is an empirical ionicity factor defined to be 0.50 for silicates and oxides, and observed to be ~0.75 for all halides, 0.40 for chalcogenides, 0.25 for phosphides and arsenides, and 0.20 for nitrides and carbides.

This equation is physically reasonable. If bond strength is zero between two atoms (i.e. $n = 0$ in Eqn. 10), as in the case of an inert gas, then thermal expansion is infinite. If bond strength is very large, as in the case of a silicon-oxygen bond, then thermal expansion approaches zero. In practice, Equation (10) may be used to predict linear expansion coefficients for average cation-anion bonds in most coordination groups to within ±20%. The formula does not work well for the largest alkali sites, for which coordination number may not be well defined. The formula is also inadequate for bond strengths greater than 0.75, which are observed to have expansion coefficients less than those predicted. Yet another limitation of this inverse relationship between bond strength and thermal expansion is the lack of information on thermal corrections to bond distances. Actual expansion coefficients must be somewhat larger than those typically cited for uncorrected bond distances. Furthermore, the strongest and shortest bonds are the ones that require the greatest thermal correction.

In the mineralogically important case when oxygen is the anion, Equation (10) reduces to:

$$\alpha_{1000} = 4.0(4)\left[\frac{\mathrm{n}}{\mathrm{z_c}}\right] \times 10^{-6}\,\mathrm{K}^{-1} \tag{11}$$

This simple relationship predicts relatively small linear thermal expansion for Si-O bonds in SiO_4 tetrahedra ($\sim 4 \times 10^{-6}$ K^{-1}), larger thermal expansion for bonds in trivalent cation octahedra such as AlO_6 ($\sim 8 \times 10^{-6}$ K^{-1}), and larger values for bonds in divalent cation octahedra such as MgO_6 ($\sim 12 \times 10^{-6}$ K^{-1}). While admittedly simplistic and empirically based, this relation provides a useful first-order estimate of cation-anion bond thermal expansion, and thus may serve as a benchmark for the evaluation of new high-temperature structural data.

The case of negative thermal expansion. The mean separation of two atoms invariably increases with increased thermal vibrations. Nevertheless, as noted in the earlier section on thermal corrections to bond distances, uncorrected interatomic distances based on fractional coordinates may be significantly shorter than the mean separation. In the case of rigidly bonded atoms that undergo significant thermal motion, this situation may result in negative thermal expansion of the structure (e.g. Cahn 1997).

Consider, for example, a silicate tetrahedral framework with relatively rigid Si-O bonds, but relatively flexible Si-O-Si linkages. Increased thermal vibrations of the bridging O atom may increase the average Si-O-Si angle, decrease R(SiO) and, consequently, reduce the mean Si-Si separation, thus imparting a negative bulk thermal expansion to the crystal.

CHANGES IN BOND DISTANCE: COMPRESSIBILITY

The work, W, done when a force per unit area or pressure, P, acts on a volume, V, is given by the familiar expression:

$$W = -P\Delta V \tag{12}$$

Both work and pressure are positive, so ΔV is constrained to be negative in all materials under compression. The magnitude of these changes is directly related to interatomic forces, so an analysis of structural changes with pressure may reveal much about these forces.

Compressibility and bulk modulus. Compressibility, or the coefficient of pressure expansion, β in units of GPa^{-1}, is defined in a way analogous to the coefficient of thermal expansion (Eqns. 6, 7 and 8):

$$\text{Linear } \beta_d = \frac{1}{d}\left(\frac{\partial d}{\partial P}\right)_T \tag{13}$$

$$\text{Volume } \beta_v = \frac{1}{V}\left(\frac{\partial V}{\partial P}\right)_T \tag{14}$$

$$\text{Mean } \beta(P_1,P_2) = \frac{2}{(\mathrm{d}_1 + \mathrm{d}_2)}\left[\frac{(\mathrm{d}_2 - \mathrm{d}_1)}{(\mathrm{P}_2 - \mathrm{P}_1)}\right] \approx \beta(P_1 - P_2)/2 \tag{15}$$

The compressibility of any linear or volume element of a crystal structure may thus be determined. The standard procedure for analyzing structural variations with pressure, therefore, is to highlight the compressibility of specific cation-anion bonds or volume elements that undergo significant change.

An important parameter that relates the change of volume with pressure is the bulk modulus, K in units of GPa, which is simply the inverse of volume compressibility:

$$K = \beta_V^{-1} \tag{16}$$

Some authors of high-pressure structural studies have also converted changes in bond distances or other linear element into "linearized bulk moduli" or "effective bulk modulus," which are defined as:

$$K_l = 3\beta_l^{-1} \tag{17}$$

This fictive property facilitates direct comparison of linear changes within a volume element of a structure (e.g. a cation coordination polyhedron) with the bulk modulus of that volume element. This parameter also provides a way to compare the compression behavior of 2- and 3-coordinated cations with those of volume elements in a structure. For the record, however, in the description of structural variations with pressure we generally favor the use of linear and volume compressibilities, which require no special mathematical manipulation and are based on the intuitively accessible concept of a fractional change per GPa.

Systematic variations of bond distance with pressure. An important observation of high-pressure structure studies is that the average cation-anion bond compression in a

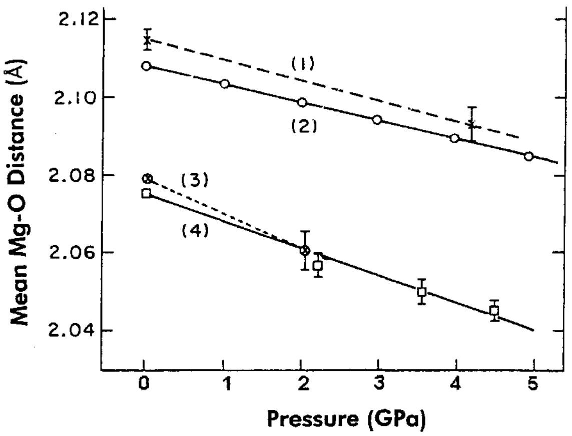

Figure 6. Mean Mg-O distances in MgO_6 octahedra versus pressure for several oxides and silicates (after Hazen and Finger 1982).

Table 1. Bulk moduli of MgO_6 octahedra in oxides and silicates

PHASE	*FORMULA*	*K (GPa)*	*Reference*
Periclase	MgO	160(2)	Hazen (1976b)
Karrooite	$MgTi_2O_5$	168(2)	Yang & Hazen (1999)
Forsterite	Mg_2SiO_4	135(15)	Hazen (1976a)
Monticellite	$CaMgSiO_4$	150(10)	Sharp et al. (1987)
Wadsleyite	γ-Mg_2SiO_4	145(8)	Hazen et al. (2000)
Diopside	$CaMgSi_2O_6$	135(20)	Levien & Prewitt (1981)

Table 2. Bulk moduli of AlO_6 octahedra in oxides and silicates

PHASE	*FORMULA*	*K (GPa)*	*Reference*
Corundum	Al_2O_3	254(2)	Finger & Hazen (1978)
Spinel	$MgAl_2O_4$	260(40)	Finger et al. (1986)
Pyrope	$Mg_3Al_2Si_3O_{12}$	211(15)	Zhang et al. (1998)
Grossular	$Ca_3Al_2Si_3O_{12}$	220(50)	Hazen & Finger (1978)
Kyanite	Al_2SiO_5	245(40)	Yang et al. (1997b)

given type of cation coordination polyhedron is usually, to a first approximation, independent of the structure in which it is found. Magnesium-oxygen (MgO_6) octahedra in MgO, orthosilicates, layer silicates, and chain silicates, for example, all have polyhedral bulk moduli within ±10% of 150 GPa (Fig. 6, Table 1). Similarly, the bulk moduli of aluminum-oxygen (AlO_6) octahedra in many structures are within ±10% of 235 GPa (Table 2). This observed constancy of average cation-anion compression is especially remarkable, because individual bonds within a polyhedron may show a wide range of compressibilities, as will be discussed below.

For silicate (SiO_4) tetrahedra, the observed compressions in most high-pressure structure studies, particularly for studies to pressures less than about 5 GPa, are on the same order as the experimental errors. This situation means that many studies of structural compression can only give a lower bound of the silicate tetrahedral bulk modulus. A significant exception is the study of pyrope by Zhang et al. (1998), who achieved very high pressure with a He pressure fluid pressure medium. These authors derived a bulk modulus for the Si site of 580±24 GPa, which provides the best constraint available to date on the compression of silicate tetrahedra.

Numerous additional examples of observed polyhedral bulk moduli are recorded in later chapters of this volume. These data provide the basis for development of empirical bond distance-pressure relationships.

Bond distance-pressure relationships. Percy Bridgman (1923) was perhaps the first researcher to attempt an empirical expression for the prediction of crystal bulk moduli and, by implication, bond compressibilities. In his classic study of the compression of 30 metals, he found that compressibility was proportional to the 4/3rds power of molar volume. The importance of mineral bulk moduli in modeling the solid Earth led Orson Anderson and his coworkers (Anderson and Nafe 1965, Anderson and Anderson 1970, Anderson 1972) to adapt Bridgman's treatment to mineral-like compounds. For isostructural materials, it is found that compressibility is proportional to molar volume, or, as expressed in Anderson's papers:

$$\text{Bulk Modulus} \times \text{Volume} = \text{constant} \tag{18}$$

A different constant is required for each isoelectronic structure type. Although this relationship is empirical, theoretical arguments in support of constant KV may be derived from a simple two-term bonding potential (Anderson 1972).

The same theoretical arguments used to explain the observed KV relationship in isostructural compounds may be used to predict a bulk modulus-volume relationship for cation coordination polyhedra. Hazen and Prewitt (1977a) found such an empirical trend in cation polyhedra from oxides and silicates:

$$\frac{K_p d^3}{z_c} = \text{constant} \tag{19}$$

where z_c is the cation formal charge, d is the cation-anion mean bond distance, and K_p is the polyhedral bulk modulus. This expression indicates that structural changes with pressure are closely related to polyhedral volume (i.e. d^3), but are essentially independent of cation coordination number or mass. Using molecular orbital techniques, Hill et al. (1994) determined bond stretching force constants for a number of nitride, oxide and sulfide polyhedra in molecules and crystals. These force constants were then employed to successfully reproduce Equation (19). Hazen and Finger (1979, 1982) summarized compression data for numerous oxides and silicates and proposed the constant:

$$\frac{K_p d^3}{z_c} \approx 750 \pm 20 \text{ GPa Å}^3 \tag{20}$$

Experimentally, the best numerical values of the polyhedral bulk moduli are obtained for the most compliant polyhedra. Therefore, small values of the bulk modulus have the greatest precision.

Studies of compounds with anions other than oxygen reveal that different constants are required. Thus, for example, Hazen and Finger (1982) systematized polyhedral bulk moduli in numerous halides (including fluorides, chlorides, bromides, and iodides) with the expression:

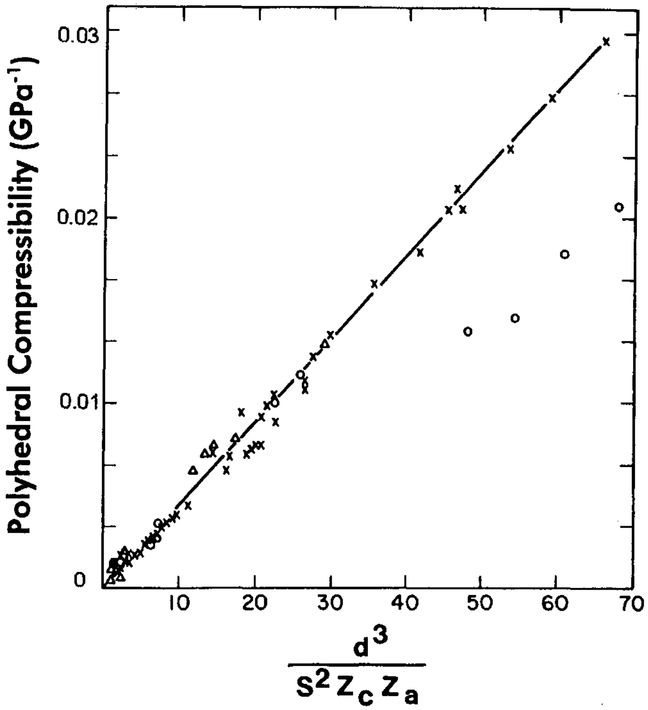

Figure 7. The polyhedral bulk modulus–volume relationsip (Eqn. 28). Polyhedral compressiblity is the inverse of polyhedral bulk modulus. The expression $d^3/S^2 z_c z_a$ is an empirical term, where d is the cation-anion bond distance, S is an ionicity term (see text), and z_c and z_a are the cation and anion formal charges, respectively. Data are indicated by Δ = tetrahedra, ☐ = octahedra, ○ = 8-coordinated polyhedra. The line is a weighted linear-regression fit constrained to pass through the origin of all data tabulated by Hazen and Finger (1979). Four circles corresponding to CsCl-type compounds fall significantly below the line, as discussed in Hazen and Finger (1982).

$$\frac{K_P d^3}{z_c} \approx 560 \pm 10 \text{ GPa Å}^3 \tag{21}$$

A more general bulk modulus-volume expression is also provided by Hazen and Finger (1982):

$$\frac{K_P d^3}{S^2 z_c z_a} \approx 750 \text{ GPa Å}^3 \tag{22}$$

where z_a is the formal anionic charge and S^2 is the same empirical "ionicity" term described previously in the empirical expression for bond thermal expansivity. This relationship is illustrated in Figure 7. Values of S^2 are 0.5 for oxides and silicates; 0.75 for halides; 0.40 for sulfides, selenides and tellurides; 0.25 for phosphides, arsenides and antimonides; and 0.20 for carbides and nitrides. It is intriguing that, while the physical significance of S^2 is not obvious, the same values apply to the independent formulations of bond compressibility and thermal expansivity.

Anomalous bond compressibilities. While cation-anion bonds in most crystal structures conform to the empirical bulk modulus-volume relationship, numerous significant anomalies have been documented, as well. These anomalies, which provide important insights to the nature of crystal compression, fall into several categories.

1. *Differences in Bonding Character*: Hazen and Finger (1982) noted a number of these anomalies, including the ZnO_4 tetrahedron in zincite (ZnO) and the VO_6 octahedron in V_2O_3, an unusual oxide with metallic luster. These polyhedra, which are significantly more compressible than predicted by Equation (22), may also be characterized by more covalent bonding than many other oxides and silicates. This observation suggests that the empirical ionicity term, S^2, may be less than 0.50 for some oxygen-based structures.
2. *Overbonded or Underbonded Anions*: The most common bond distance-compression anomalies occur in distorted polyhedra in which one or more coordinating anion is significantly overbonded or underbonded. A typical example is provided by the Al1 octahedron in sillimanite (Al_2SiO_5), which was studied at pressure by Yang et al. (1997a). This centric polyhedron has two unusually long 1.954 Å bonds between Al1 and the extremely overbonded OD oxygen, which is coordinated to one ^{IV}Si, one ^{IV}Al and one ^{VI}Al. The compressibility of Al1-OD is twice that of other Al-O bonds (Fig. 8), yielding a polyhedral bulk modulus of 162±8 GPa. This value is significantly less than the predicted 300 GPa value (Eqn. 22) and the observed 235±25 GPa value typical of other oxides and silicates (Table 2).

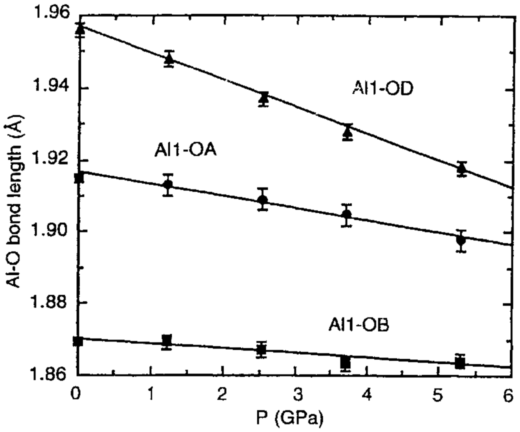

Figure 8. Al-O distances versus pressure in sillimanite (after Yang et al. 1997a).

A similar situation occurs in the Mg2 octahedron of orthoenstatite ($MgSiO_3$), which was investigated at high-pressure by Hugh-Jones and Angel (1994). The unusually long bond (2.46 Å) between Mg2 and overbonded O3B compresses a remarkable 8% between room pressure and 8 GPa (Fig. 9). This anomalous Mg2-O3B bond compression contributes to an octahedral bulk modulus of ~60 GPa, compared to the predicted value of 160 GPa (Eqn. 22) and typical observed 150±15 GPa values for other MgO_6 groups (Table 1). This bond distance, furthermore, displays a pronounced curvature versus pressure—a feature rarely observed in other structures.

3. *Second-Nearest Neighbor Interactions*: Of the approximately two dozen structure types examined in developing polyhedral bulk modulus-volume relationships, halides with the cubic CsCl structure stand out as being significantly less compressible than predicted by Equation (22) (see Fig. 7). The CsCl structure, with eight anions at the corners of a unit cube, and a cation at the cube's center, is unique in the high degree of polyhedral face sharing and the consequent short cation-cation and anion-anion separations. In CsCl-type compounds the cation-cation distance is only 15% longer than cation-anion bonds, in contrast to the 50 to 75% greater separation in most other structure types. It is probable, therefore, that Equation (22), which incorporates only the bonding character of the primary coordination sphere, is not valid for structures in which extensive polyhedral face sharing results in significant second-nearest neighbor interactions.

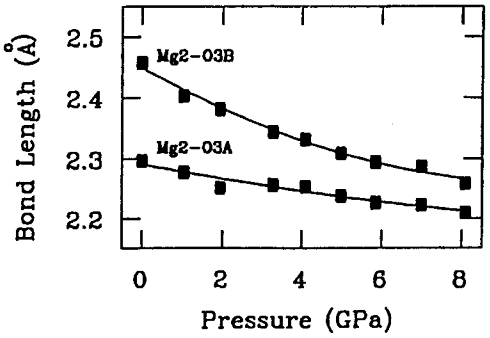

Figure 9. Mg-O distances versus pressure in orthoenstatite (after Hugh-Jones and Angel 1994).

Table 3. Bulk moduli of $Fe^{2+}O_6$ octahedra in oxides and silicates

PHASE	*FORMULA*	*K (GPa)*	*Reference*
Wüstite	$Fe_{1-x}O$	154(2)	Hazen (1981)
Ilmenite	$FeTiO_3$	140(10)	Weschler & Prewitt (1984)
Fayalite	Fe_2SiO_4	130(15)	Kudoh & Takeda (1986)
Fe-Wadsleyite	γ-Fe_2SiO_4	~150	Hazen et al. (2000)
Hedenbergite	$CaMgSi_2O_6$	150(7)	Zhang et al. (1997)
Orthoferrosilite	$Fe_2Si_2O_6$	135(10)	Hugh-Jones et al. (1997)

A subtler example of this anomalous behavior may be presented by the $Fe^{2+}O_6$ octahedron in iron silicate spinel (Fe_2SiO_4), for which high-pressure structural data were reported by Finger et al. (1979). Ferrous iron octahedra in many oxides and silicates display bulk moduli of 140±15 GPa (Table 3), in close agreement with the value of 150 GPa suggested by the polyhedral bulk modulus-volume relationship (Eqn. 22). However, the octahedron in iron silicate spinel has a significantly greater bulk modulus of 190±20 GPa. Hazen (1993) has proposed that the anomalous stiffness of this site may result from the unusually short 2.9 Å Fe-Fe separation across shared octahedral edges in this compound—a distance only about 34% longer than the Fe-O separation.

POLYHEDRAL VARIATIONS

Polyhedral volumes may be used to calculate polyhedral thermal expansivity and compressibility in the same way that temperature-volume and pressure-volume data are used to calculate equations of state (see Angel, this volume). In general, however, these expressions of approximate polyhedral volume change are also easily calculated from linear changes. For polyhedra that do not undergo severe distortion, the polyhedral thermal expansivity and compressibility are given by:

$$\alpha_v = \frac{1}{V}\left(\frac{\partial V}{\partial T}\right)_P \approx \frac{3}{d}\left(\frac{\partial d}{\partial T}\right)_P \qquad (23)$$

$$\beta_v = \frac{1}{V}\left(\frac{\partial V}{\partial P}\right)_T \approx \frac{3}{d}\left(\frac{\partial d}{\partial P}\right)_T \qquad (24)$$

where $1/d(\partial d/\partial T)$ is the mean linear thermal expansivity, etc. These relationships also allow the calculation of "effective" volumetric polyhedral parameters for a planar atomic group or for an individual bond. Thus, for example, if the mean C-O compressibility of a CO_3 group is known, then the effective polyhedral compressibility may be calculated from Equation (24).

1. A common, though by no means universal, trend is for highly distorted polyhedra to become more regular at high pressure (and more distorted at high temperature) as a consequence of differential bond compression (or thermal expansion). In numerous polyhedra, including the sillimanite and orthoenstatite examples cited above, longer bonds tend to be significantly more compressible (or expansible) than shorter bonds. Other examples of this behavior include the AlO_6 octahedron in corundum (Al_2O_3; Finger and Hazen 1978), the LiO_6 octahedron in lithium-scandium olivine ($LiScSiO_4$; Hazen et al. 1996), and all three MO_6 octahedra in wadsleyite (β-Mg_2SiO_4; Hazen et al. 2000). Thus, quadratic elongation commonly decreases with pressure (or increases with temperature).
2. Counter examples, though unusual, do arise. The shortest M1-O2 bond in the $M1O_6$ octahedron of karrooite ($MgTi_2O_5$; Yang and Hazen 1999), for example, is most compressible, whereas the longest M1-O3 bond is least compressible, though the differences in compressibility are only about 20%. This situation apparently arises from the restrictive juxtaposition of octahedral shared edges in this pseudobrookite-type structure.

Changes in interpolyhedral angles

Framework silicates such as quartz or feldspar can display large compressibilities even though individual cation-anion distances are essentially unchanged as a result of cation-anion-cation bond angle bending. The relative flexibility of such interpolyhedral angles has received considerable study, both experimental and theoretical. Downs and Palmer (1994), for instance, showed that the silica polymorphs quartz, cristobalite and coesite all displayed the same volume change for a given change in Si-O-Si angle.

Geisinger and Gibbs (1981) applied *ab initio* molecular orbital methods to document the relative energies of *T*-O-*T* angles, where *T* is a tetrahedrally-coordinated cation, such as Si, Al, B, or Be, and O is a bridging oxygen atom, either 2- or 3-coordinated. Their results, which were presented in a series of graphs of total energy versus *T*-O-*T* bond angle for H_6SiTO_7 and H_7SiTO_7 clusters, suggest that the flexibility of the angle is strongly dependent on both *T* and the oxygen coordination. They calculate, for example, that *T*-O-*T* angles with a third cation coordinated to the bridging oxygen are much more rigid than for angles with two-coordinated oxygen. Si-O-Al and Si-O-B angles, furthermore, tend to be more flexible than Si-O-Si angles.

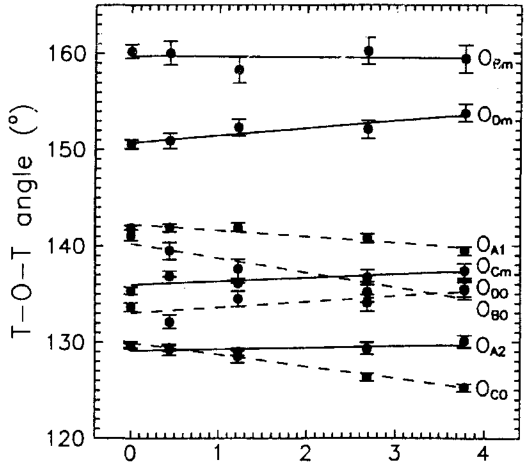

Figure 10. Si-O-*T* angles in albite versus pressure (from Downs et al. 1994).

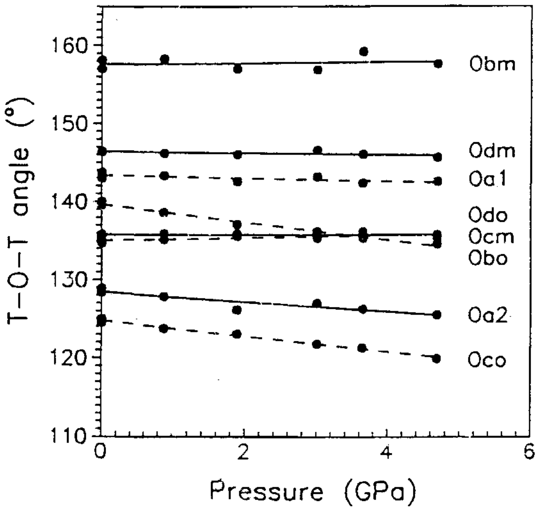

Figure 11. Si-O-*T* angles in reedmergnerite versus pressure (from Downs et al. 1999).

These theoretical predictions are largely born out by high-pressure structural studies of feldspar. In low albite ($NaAlSi_3O_8$), Downs et al. (1994) observed that the greatest decreases in Si-O-*T* angles occur for the Si-OCO-Al and Si-OBO-Al angles, whereas all Si-O-Si angles show essentially no decrease with increasing pressure (Fig. 10). Similarly, in reedmergnerite ($NaBSi_3O_8$), Downs et al. (1999) reported that Si-OCO-B and Si-OBO-B angles undergo the greatest decrease with pressure (Fig. 11). Furthermore, microcline ($KAlSi_3O_8$), with a larger molar volume than albite, has a larger bulk modulus than albite. This result is in disagreement with the trends suggested by Bridgman (1923) and Equation (24). Downs et al. (1999) suggest that the cause of this discrepancy is that all the bridging bonds in microcline are bonded to the large K cation, while this is not the case in albite with the smaller Na cation. Consequently, the bridging Si-O-*T* angles are stiffer in microcline. In spite of these qualitative trends, however, no quantitative estimates of bond angle bending, and associated compression, have yet been proposed.

VARIATION OF TEMPERATURE FACTORS WITH PRESSURE

Finger and King (1978) demonstrated that pressure has a small, but possibly measurable, effect on the isotropic temperature factor. The average energy, E, associated with a vibrating bond of mean ionic separation, d, and mean-square displacement $<r^2>$, ($r \ll d$), is:

$$E \approx \frac{z_c z_a e^2}{2d^3}(ad-2) <r^2> \tag{25}$$

where z_c and z_a are cation and anion charges, and a is a repulsion parameter (Karplus and Porter 1970). The isotropic temperature factor, B, is proportional to the mean-square displacement:

$$B = 8\pi^2 <r^2> \tag{26}$$

Therefore, combining Equations (25) and (26),

$$E = \frac{z_c z_a e^2 B}{16\pi^2 d^3}(ad-2) \tag{27}$$

If it is assumed that the average energy, E, and the repulsion parameter, a, are independent of pressure, then the temperature factor at pressure, B_P, is related to the room-pressure temperature factor, B_0, as follows:

$$B_P = B_0 \frac{(ad_0 - 2)d_P^3}{(ad_P - 2)d_0^3} \tag{28}$$

In the case of NaCl at 3.2 GPa, Finger and King (1978) predicted a 5.7% reduction in the temperature factors of Na and Cl at high pressure. The observed reductions of approximately 10±5% provided evidence for the proposed effect of pressure on amplitude of atomic vibrations.

DISTORTION INDICES BASED ON CLOSE PACKING

Thompson and Downs (1999, 2001) have proposed that the temperature or pressure variations of structures based on approximately close-packing of anions can be described in terms of closest-packing systematics. A parameter, U_{CP}, that quantifies the distortion of the anion skeleton in a crystal from ideal closest-packing is calculated by comparing the observed anion arrangement to an ideal packing of the same average anion-anion separation. Thus, U_{CP} is a measure of the average isotropic displacement of the observed anions from their ideal equivalents. An ideal closest-packed structure can be fit to an observed structure by varying the radius of the ideal spheres, orientation, and translation, such that U_{CP} is minimized. Thompson and Downs fit ideal structures to the $M1M2TO_4$ polymorphs, pyroxenes, and kyanite. They analyzed the distortions of these crystals in terms of the two parameters, U_{CP} and the ideal radius, and characterized changes in structures due to temperature, pressure, and composition in terms of these parameters. In general, they propose that structures that are distorted from closest-packing will show a decrease in both U_{CP} and oxygen radius with pressure, while structures that are already closest-packed will only compress by decreasing the oxygen radius.

COMPARISONS OF STRUCTURAL VARIATIONS WITH TEMPERATURE AND PRESSURE

Hazen (1977) proposed that temperature, pressure and composition may behave as structurally analogous variables in structures where atomic topology is primarily a function of molar volume. Subsequent crystallographic studies have demonstrated that, while this relationship holds for some simple structure types, most structures display more complex behavior. In these cases, deviations from the "ideal" behavior may provide useful insights regarding structure and bonding. In the following section, therefore, we review the structural analogy of temperature, pressure and composition, and examine the so-called "inverse relationship" between temperature and pressure, as originally proposed by Hazen (1977) and Hazen and Finger (1982).

Structurally analogous variables

Hazen (1977) proposed that geometrical aspects of structure variation with temperature, pressure or composition are analogous in the following ways:

1. The fundamental unit of structure for the purposes of the analogy is the cation coordination polyhedron. For a given type of cation polyhedron, a given change in temperature, pressure or composition (*T*, *P* or *X*) has a constant effect on polyhedral size, regardless of the way in which polyhedra are linked. Polyhedral volume coefficients α_v, β_v and γ_v are thus independent of structure to a first approximation. We have seen above that in the case of α_v and β_v these polyhedral coefficients are similar to about ±10% in many compounds, but that significant anomalies are not uncommon.

2. Polyhedral volume changes with *T*, *P* or *X* may be estimated from basic structure and bonding parameters: cation-anion distance (*d*), cation radius (*r*), formal cation and anion charge (z_c and z_a) and an ionicity term (S^2).

$$\alpha_v = \frac{1}{V}\left(\frac{\partial V}{\partial T}\right) \approx 12.0\left(\frac{n}{S^2 z_c z_a}\right) 10^{-6}\,\mathrm{K}^{-1} \tag{29}$$

$$\beta_v = \frac{1}{V}\left(\frac{\partial V}{\partial P}\right) \approx 0.00133\left(\frac{d^3}{S^2 z_c z_a}\right)\mathrm{GPa}^{-1} \tag{30}$$

$$\gamma_v = \frac{1}{V}\left(\frac{\partial V}{\partial X}\right) \approx \frac{3(r_2 - r_1)}{d} \tag{31}$$

3. As a corollary, in structures with more than one type of cation polyhedron, variations of *T*, *P* or *X* all have the effect of changing the ratios of polyhedral sizes.

T-P-X surfaces of constant structure

All crystalline materials may be represented in *T-P-X* space by surfaces of constant molar volume (isochoric surfaces). One consequence of the structural analogy of temperature, pressure and composition is that for many substances isochoric surfaces are also surfaces of constant structure in *T-P-X* space (Hazen 1977). Consider, for example, the simple fixed structure of the solid solution between stoichiometric MgO and FeO. A single parameter, the unit-cell edge, completely defines the structure of this NaCl-type compound. Isochoric surfaces are constrained to be isostructural surfaces in *T-P-X* space (Fig. 12), because variations in temperature, pressure or composition all change this parameter. Isochoric or isostructural surfaces may be approximately planar over a limited

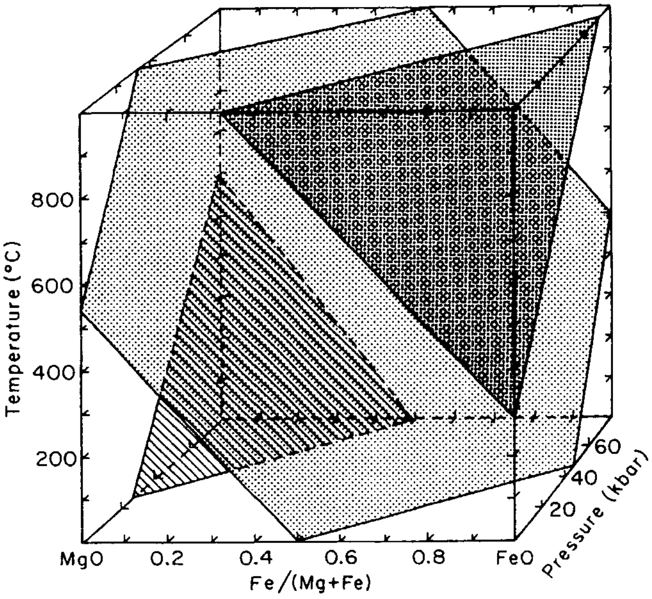

Figure 12. Isostructural surfaces for (Mg,Fe)O in *T-P-X* space (after Hazen and Finger 1982).

range of temperature, pressure and composition; however, α_v, β_v, and γ_v generally vary with *T, P* and *X*, thus implying curved surfaces of constant volume.

Isostructural surfaces exist for a large number of compounds. The Mg-Fe silicate spinel, γ-$(Mg,Fe)_2SiO_4$, for example, has a cubic structure with only two variable parameters—the unit cell edge and the *u* fractional coordinate of oxygen. In this case, the structure is completely defined by the two cation-oxygen bond distances: octahedral (Mg,Fe)-O and tetrahedral Si-O. The size of the silicon tetrahedron is relatively constant with temperature, pressure and Fe/Mg octahedral composition. Consequently, isostructural *T-P-X* surfaces for the octahedral component of the silicate spinels will also approximate planes of constant spinel structure. Note that the isostructural surfaces of Mg-Fe oxide and silicate spinel will be similar because both depend primarily on the size of the (Mg,Fe) octahedron.

All isostructural surfaces have certain features in common. Consider the slopes of such a surface:

$$\left(\frac{\partial P}{\partial T}\right)_{S,X}, \left(\frac{\partial P}{\partial X}\right)_{S,T} \text{ and } \left(\frac{\partial T}{\partial X}\right)_{S,P} \tag{32}$$

where *S* designates partial differentials at constant structure (as well as constant molar volume), and $+\partial X$ is defined as substitution of a larger cation for a smaller one. It follows that:

$$\left(\frac{\partial P}{\partial T}\right)_{S,X} > 0 \quad (33) \qquad \left(\frac{\partial P}{\partial X}\right)_{S,T} > 0 \quad (34) \qquad \left(\frac{\partial T}{\partial X}\right)_{S,P} < 0 \quad (35)$$

Even relatively complex structures, such as the biaxial alkali feldspars,

$(K,Na)AlSi_3O_8$, may have *T-P-X* surfaces that approximate isostructural surfaces (Hazen 1976c). By contrast, however, in many structures with more than two different types of cation polyhedra, a given change in *T*, *P* or *X* will commonly not be cancelled by any possible combination of changes of the other two variables, unless multiple chemical substitutions are invoked. For example, the cell parameters of calcite, $CaCO_3$, display unique values at all combinations of P and T, making it an ideal *in situ* thermometer and barometer. Multiple compositional variables, of course, increase the dimensions of the *T-P-X* space under consideration.

THE INVERSE RELATIONSHIP BETWEEN COMPRESSION AND THERMAL EXPANSION

In numerous structures, geometrical changes upon cooling from high temperature are similar to those upon compression. In other words, structural variations due to changes in temperature may be offset by variations due to changes in pressure (Fig. 13). This common type of structural behavior, as first observed in sanidine (Hazen 1976c), and illustrated in Figure 14 for the *u* parameter of silicate spinels, Figure 15 for the unit-cell axes of chrysoberyl, and Figure 16 for the unit-cell parameters of low albite, has been called the "inverse relationship" by Hazen and Finger (1982). The inverse relationship may obtain when:

1. All polyhedra in a structure have similar ratios of expansivity to compressibility; i.e. α/β is a constant for all polyhedra of the structure; or,
2. One polyhedron is relatively rigid (α and β are small) compared to the other polyhedra, which have similar α/β.

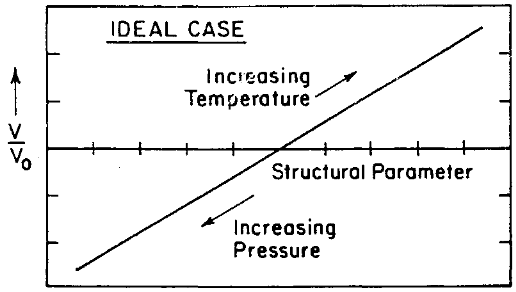

Figure 13. The idealized inverse effect of temperature and pressure on structure (after Hazen and Finger 1982).

These conditions are fulfilled by numerous compounds, including most materials with only one type of cation polyhedron, and many silicates with only one type of polyhedron other than the relatively rigid Si tetrahedra. From Equations (29) and (30) for polyhedral α and β:

$$\frac{\alpha}{\beta} \approx 90\left(\frac{n}{d^3}\right)\text{bar/°C} \qquad (36)$$

Thus, the "inverse relationship" should obtain if n/d^3 is similar for all cation polyhedra in a structure. Coincidentally, several common polyhedra in rock-forming minerals have similar observed ratios of α to β. Octahedral Mg, Fe^{2+}, Al and Fe^{3+} all have $\alpha/\beta \approx 65$ bar/°C. Thus many minerals display the inverse relationship. Values of predicted α and β for many common cation polyhedra are illustrated in Figure 17.

Note that the pressure required to offset a 1°C increase in temperature is not the same for all compounds. In the case of MgO and Mg_2SiO_4, approximately 75 bars offset

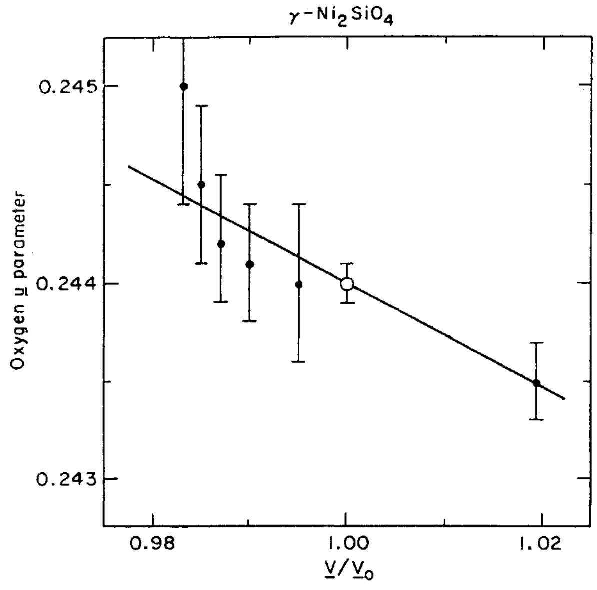

Figure 14 (above). The u parameter of nickel silicate spinel versus V/V_0 (after Hazen and Finger 1987).

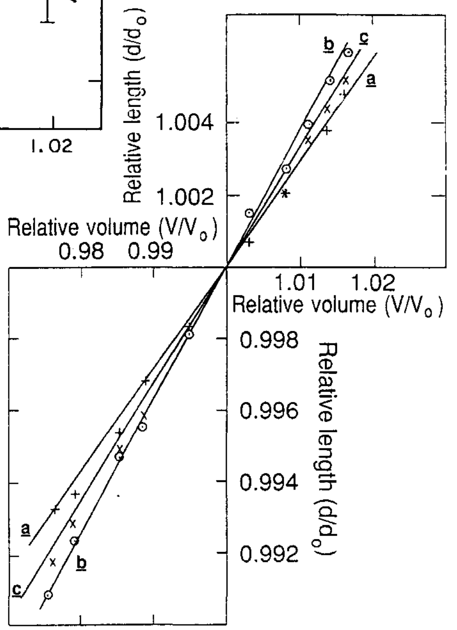

Figure 15 (right). Unit-cell dimensions of chrysoberyl versus temperature and pressure (after Hazen and Finger 1987).

1°C, while alkali feldspar ($NaAlSi_3O_8$) requires only 20 bars to offset 1°C. Note that $(\partial P/\partial T)_S$ for many minerals is greater than the average 25 bar/°C geotherm of the Earth's crust and upper mantle. Thus many common minerals have greater molar volumes at depth in the Earth than at the surface.

Rutile remains a curious exception to the ideal inverse relationship. Rutile-type TiO_2 is tetragonal with only one type of polyhedron ($^{VI}Ti^{4+}$). Rutile should follow the trend observed in other simple oxides, but a plot of the axial ratio c/a versus V/V_0 (Fig. 18) shows a more complex behavior: c/a increases *both* with T and P. Surveys of several rutile-type compounds at temperature (Rao 1974) and pressure (Hazen and Finger 1981) reveal that although most isomorphs have increasing c/a with pressure, the temperature response is highly variable. Therefore, the temperature variation of rutile-type compounds is not controlled by structure, because all of these compounds have the same polyhedral arrangement.

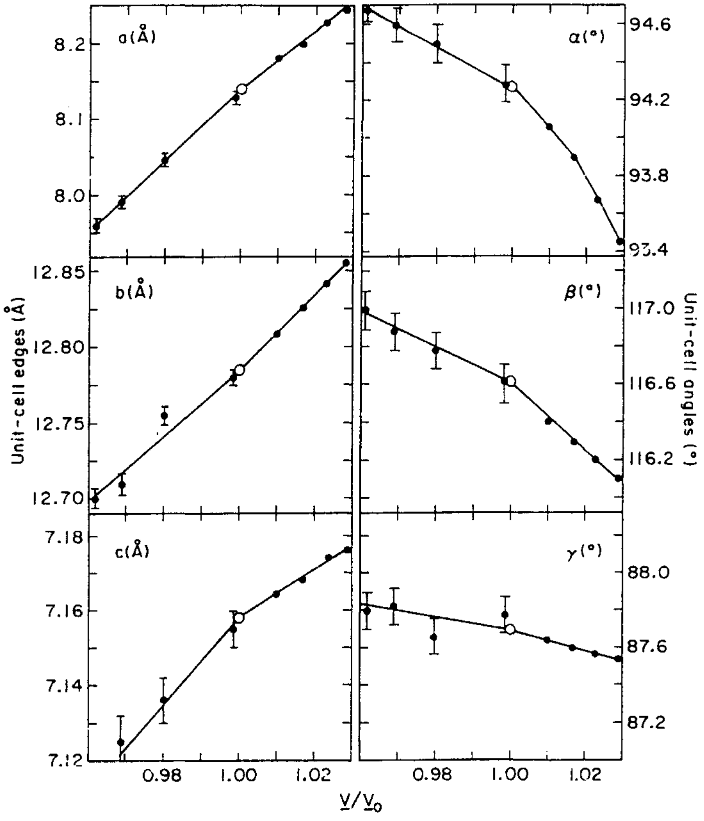

Figure 16. Unit-cell parameters of low albite versus V/V_0 (after Hazen and Prewitt 1977b).

OPPORTUNITIES FOR FUTURE RESEARCH

In spite of the growing body of data on crystal structure variations with temperature and pressure, our general understanding of comparative crystal chemistry remains at a largely empirical state. Significant opportunities exist for advancing the field, both experimentally and theoretically. A few of these promising research areas are outlined below.

Interatomic potentials

The pressure response of crystal structures provides direct information about bonding potential. Consider, for example, a simple two-term expression for the total bond potential energy, U, between a cation and anion:

$$U_{bond} = \frac{z_c z_a e^2}{d} + \frac{B}{d^n} \qquad (37)$$

where e is the charge on an electron, d is the cation-anion distance, and B and n are repulsive energy constants that depend on the electronic structure of the two ions. Total site energy, the energy required to separate a particular ion, j, to an infinite separation

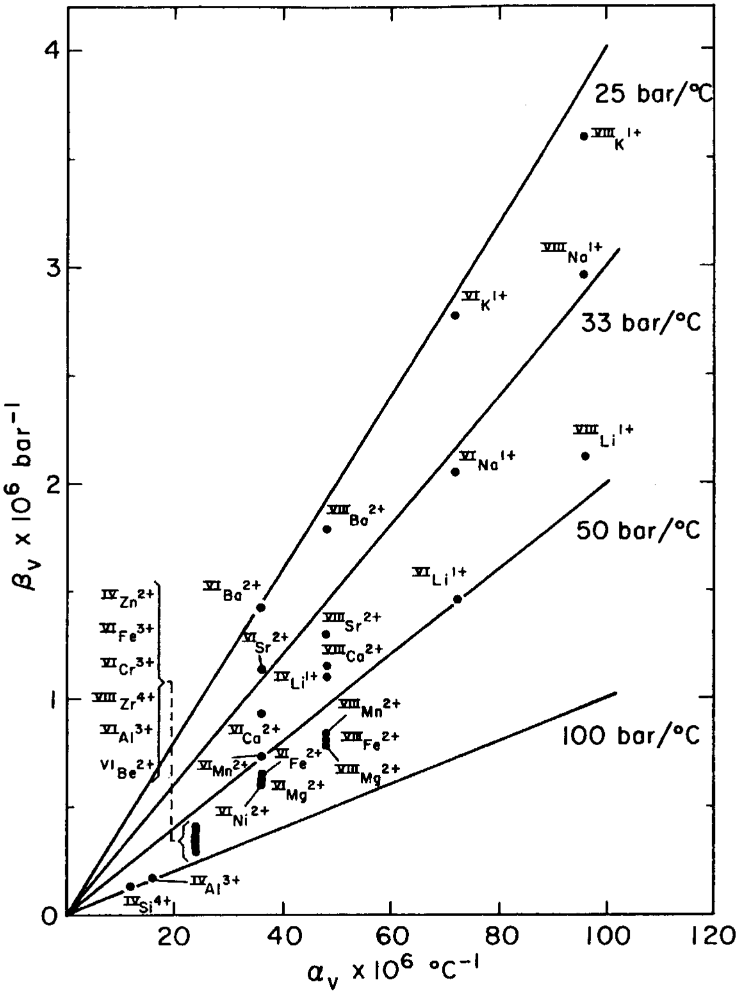

Figure 17. α versus β for oxygen-based polyhedra (after Hazen and Prewitt 1977a).

from its equilibrium position in a crystal, is then given by the sum of an attractive and a repulsive term:

$$U_j = \frac{A_j e^2}{d_j} + \sum_i^N B_{ij} / d_{ij}^{nj} \tag{38}$$

where A_j is the dimensionless Madelung constant (e.g. Ohashi and Burnham 1972), which must be calculated for each site, and d_j is the nearest-neighbor cation-anion distance.

If a pressure acts on a cross-sectional area approximately equal to the square of the interatomic distance (d^2) then the net force on the bond is $F_P = Pd^2$. At equilibrium distance the sum of the bonding forces is zero:

$$\frac{\partial U_j}{\partial d_j} + F_p = 0 \tag{39}$$

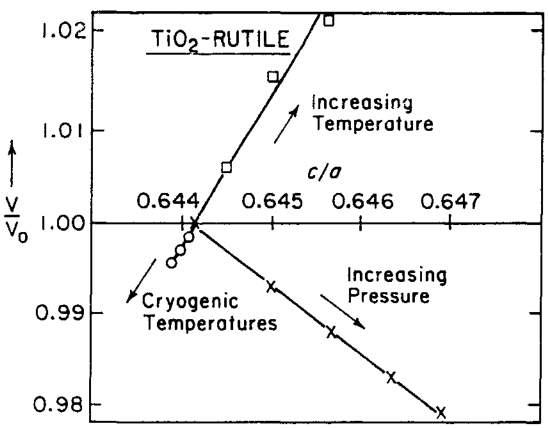

Figure 18. Axial ratio *c/a* for rutile (TiO_2) versus V/V_0. The *c/a* of rutile does not follow the inverse relationship, because the ratio increases with both *T* and *P* (after Hazen and Finger 1981).

Combining this expression with Equation (37):

$$\frac{A_j e^2}{d_j^2} - \frac{nB}{d^{(n+1)}} + P d_j^2 = 0 \qquad (40)$$

or,

$$P = \frac{nB}{d_j^{(n+3)}} - \frac{A_j e^2}{d_j^4} \qquad (41)$$

Therefore,

$$-\frac{1}{d}\left(\frac{\partial \mathrm{d}}{\partial \mathrm{P}}\right) = \frac{1/(n+3)}{P + [(n-1)/(n+3)]\left(\frac{Ae^2}{d_j^4}\right)} \qquad (42)$$

Thus, if values of bonding parameters n, B, d_j and A_j are known, then bond compressibility may be calculated. Conversely, it may be possible to derive these or other empirical bonding parameters from bond compressibility data. To our knowledge, only Waser and Pauling (1950) have undertaken a systematic effort to extract this sort of bonding information from high-pressure structure data.

Molecular structures and intermolecular forces

Hazen and Finger (1985) suggested that three principal compression mechanisms—bond compression, cation-anion-cation bond angle bending, and intermolecular compression—account for most volume change in crystals. Most previous high-pressure or high-temperature structure studies have focused on dense, mineral-like compounds, in which bond compression and angle bending are the dominant compression mechanisms. Much less effort has been devoted to molecular crystals, though the body of work on condensed molecular crystals, particularly at high pressure is growing (see Hemley and Dera, this volume).

An opportunity thus exists both for systematic studies of molecular crystals under pressure, and for a general synthesis of the behavior of these phases at extreme conditions.

Additional physical properties

Although the most definitive measurements on high-pressure phases are obtained from diffraction measurements, other techniques can provide additional information that often is essential for understanding crystal behavior in the high pressure-temperature regime. Among the most useful techniques are various forms of spectroscopy, including Raman, infrared, and Mössbauer. These tools are being used in many laboratories to detect phase transitions and can provide information about short-range interactions that are masked in diffraction studies, which focus on longer-range properties of materials. Much future research will depend on integration of all of these techniques to give a broad picture of how minerals and their analogs behave as functions of pressure and temperature.

Another spectroscopic technique that has been used recently to give additional crystal-chemical information about iron oxides and sulfides at high pressure is X-ray spectroscopy. In this technique, synchrotron X-rays are used to explore whether the Fe$K\beta$ peak is present in the spectra from iron oxide specimens. If it is present, the iron in the sample is assumed to be in the high-spin state; if it is absent, then iron is in the low-spin state. The primary crystal-chemical result is that the interatomic distances are different in the two situations and this difference, in turn, reveals how the material is responding to pressure and/or temperature changes. An example of the application of this spectroscopy to FeO is described by Badro et al. (1999).

Synchrotron-related research

Mao and Hemley (1998) reviewed the wide range of experiments that are being conducted under high pressures and temperatures and illustrated some of the new opportunities that are now open through the use of synchrotron radiation. The availability of synchrotron sources to the geosciences high-pressure community as well as to those in materials science and physics is having a major impact on the field and is enabling many different kinds of experiments that heretofore were impossible.

Powder diffraction. Diffraction experiments are now possible on polycrystalline samples to pressures in the megabar range and temperatures of thousand of degrees. This extended experimental range is made possible by new diamond-anvil cell designs together with laser heating of the samples. Further advances are being made in recording diffraction patterns in real time along with pressure and temperature applications. One problem often encountered in these experiments is that it is difficult to characterize completely the crystal structures of the phase or phases that appear as pressure and temperature increase. Because the diffraction patterns are often not of high quality and it is difficult to know if the sample is single- or multiple-phase, identification of the crystal structure can be a complex procedure. An example of this problem is the high-pressure structure of Fe_2O_3. Staun Olsen et al. (1991) reported the structure of Fe_2O_3 above 50 GPa to be orthorhombic perovskite, but later work by Pasternak et al. (1999) using both X-ray diffraction and Mössbauer spectroscopy maintains that the structure type is Rh_2O_3 II (Shannon and Prewitt 1970). The problem is that the calculated diffraction patterns for these two possible structures are almost identical and it is thus very difficult to distinguish between them with poor quality X-ray data. Another complication is that, even if the phase in question does have the same structure as an ambient-pressure material, its lattice parameters may be very different. Thus, it will be necessary to develop better instrumental techniques and more versatile computer software in order to solve these problems.

Single-crystal diffraction. One of the most important frontiers in high-temperature and high-pressure crystal chemistry is the expansion of experimental environments to greater extremes. For most of the past 25 years, the limit for single-crystal high-pressure experiments was about 10 GPa because the beryllium backing plates used in the Merrill-Bassett diamond cell would fail at that pressure. New cell designs and higher-energy X-rays available at synchrotrons, however, are leading the way to experiments at 50 GPa and higher (Allan et al. 1996, Zhang et al. 1998, Miletich et al. 1999). With appropriate instrumentation, software, and human effort, it should be possible to conduct a whole new range of high-pressure experiments and to obtain unambiguous information about the variation of crystal structures at these extreme conditions.

REFERENCES

Allan DR, Miletich R, Angel RJ (1996) A diamond-anvil cell for single-crystal X-ray diffraction studies to pressures in excess of 10 GPa. Rev Sci Instr 67:840-842

Anderson OL, Nafe JE (1965) The bulk modulus-volume relationship for oxide compounds and related geophysical problems. J Geophys Res 70:3951-3963

Anderson DL, Anderson OL (1970) The bulk modulus-volume relationship for oxides. J Geophys Res 75:3494-3500

Anderson OL (1972) Patterns in elastic constants of minerals important to geophysics. *In* Nature of the Solid Earth, Robinson EC (ed) McGraw-Hill, New York, p 575-613

Badro J, Struzhkin VV, Shu J, Hemley RJ, Mao H-K (1999) Magnetism in FeO at megabar pressures from X-ray emission spectroscopy. Phys Rev Lett 83:4101-4104

Bartelmehs KL, Downs RT, Gibbs G., Boisen Jr MB, Birch JB (1995) Tetrahedral rigid-body motion in silicates. Am Mineral 80:680-690

Boisen MB, Jr., Gibbs GV (1990) Mathematical Crystallography: An Introduction to the Mathematical Foundations of Crystallography. Reviews in Mineralogy, Vol 15. Mineralogical Society of America, Washington, DC

Bridgman PW (1923) The compressibility of thirty metals as a function of temperature and pressure. Proc Am Acad Arts Sci 58:165-242

Brown GE, Jr., Mills BA (1986) High-temperature structure and crystal chemistry of hydrous alkali-rich beryl from the Harding Pegmatite, Taos County, New Mexico. Am Mineral 71:547-556

Busing WR, Levy HA (1964) The effect of thermal motion on the estimation of bond lengths from diffraction measurements. Acta Crystallogr 17:142-146

Cahn RW (1997) The how and why of thermal contraction. Nature 386:22-23

Cameron M, Sueno S, Prewitt CT, Papike JJ (1973) High-temperature crystal chemistry of acmite, diopside, hedenbergite, jadeite, spodumene, and ureyite. Am Mineral 58:594-618

Dollase WA (1974) A method of determining the distortion of coordination polyhedra. Acta Crystallogr A30:513-517

Downs JW (1983) An Experimental Examination of the Electron Density Distribution in Bromellite, BeO, and Phenacite, Be_2SiO_4. PhD Dissertation, Virginia Polytech Inst & State Univ, Blacksburg, VA

Downs JW, Ross FK, Gibbs GV (1985) The effects of extinction on the refined structural parameters of crystalline BeO: a neutron and X-ray diffraction study. Acta Crystallogr B41:425-431

Downs RT, Hazen RM, Finger LW (1994) The high-pressure crystal chemistry of low albite and the origin of the pressure dependency of Al-Si ordering. Am Mineral 79:1042-1052

Downs RT, Yang H, Hazen RM, Finger LW, Prewitt CT (1999) Compresibility mechanisms of alkali feldspars: New data from reedmergnerite. Am Mineral 84:333-340

Downs RT, Palmer DC (1994) The pressure behavior of α-cristobalite. Am Mineral 79:9-14

Fei Y (1995) Thermal expansion. *In* Mineral Physics and Crystallography: A Handbook of Physical Constants, T.J.Ahrens (ed) Vol 2. American Geophysical Union, Washington. p 29-44

Finger LW, Prince E (1975) A system of Fortran IV computer programs for crystal structure determination. In US Technical Note 854. National Bureau of Standards (United States)

Finger LW, Hazen RM (1978) Crystal structure and compression of ruby to 46 kbar. J Appl Phys 49:5823-5826

Finger LW, King HE (1978) A revised method of operation of the single-crystal diamond cell and refinement of the structure of NaCl at 32 kbar. Am Mineral 63:337-342

Finger LW, Hazen RM, Yagi T (1979) Crystal structures and electron densities of nickel and iron silicate spinels at elevated temperatures and pressures. Am Mineral 64:1002-1009

Finger LW, Hazen RM (1980) Crystal structure and isothermal compression of Fe_2O_3, Cr_2O_3, and V_2O_3 to 50 kbars. J Appl Phys 51:5362-5367

Finger LW, Hazen RM, Hofmeister AM (1986) High-pressure crystal chemistry of spinel ($MgAl_2O_4$) and and magnetite (Fe_3O_4): Comparisons with silicate spinels. Phys Chem Minerals 13:215-220

Fleet ME (1976) Distortion parameters for coordination polyhedra. Mineralogical Magazine 40: 531-533.

Geisinger KL, Gibbs GV (1981) STO-3G molecular orbital (MO) calculated correlations of tetrahedral SiO and AlO bridging bond lengths with p_o and f_s. Geol Soc Am Abstr with Programs 13:458

Gibbs GV (1982) Molecules as models for bonding in silicates. Am Mineral 67:421-450

Gibbs GV, Spackman MA, Boisen Jr, MB (1992) Bonded and promolecule radii for molecules and crystals. Am Mineral 77:741-750

Hazen RM (1976a) Effects of temperature and pressure on the crystal structure of forsterite. Am Mineral 61:1280-1293

Hazen RM (1976b) Effects of temperature and pressure on the cell dimension and X-ray temperature factors of periclase. Am Mineral 61:266-271

Hazen RM (1976c) Sanidine: predicted and observed monoclinic-to-triclinic reversible transformations at high pressure. Science 194:105-107

Hazen RM (1977) Temperature, pressure, and composition: structurally analogous variables. Phys Chem Minerals 1:83-94

Hazen RM, Prewitt CT (1977a) Effects of temperature and pressure on interatomic distances in oxygen-based minerals. Am Mineral 62:309-315

Hazen RM, Prewitt CT (1977b) Linear compressibilities of low albite: high-pressure structural implications. Am Mineral 62:554-558

Hazen RM, Finger LW (1978) Crystal structures and compressibilities of pyrope and grossular to 60 kbar. Am Mineral 63:297-303

Hazen RM, Finger LW (1979) Bulk modulus-volume relationship for cation-anion polyhedra. J Geophys Res 84:6723-6728

Hazen RM (1981) Systematic variation of bulk modulus of wustite with stoichiometry. Carnegie Inst Washington Year Book 80:277-280

Hazen RM, Finger LW (1981) Bulk moduli and high-pressure crystal structures of rutile-type compounds. J Phys Chem Solids 42:143-151

Hazen RM, Finger LW (1982) Comparative Crystal Chemistry: Temperature, Pressure, Composition and the Variation of Crystal Structure. John Wiley & Sons, New York

Hazen RM, Finger LW (1985) Crystals at high pressure. Sci Am 252:110-117

Hazen RM, Finger LW (1986) High-pressure and high-temperature crystal chemistry of beryllium oxide. J Appl Phys 59:3728-3733

Hazen RM (1987) High-pressure crystal chemistry of chrysoberyl Al_2BeO_4: Insights on the origin of olivine elastic anisotropy. Phys Chem Minerals 14:13-20:

Hazen RM, Finger LW (1987) High-temperature crystal chemistry of phenakite (Be_2SiO_4) and chrysoberyl ($BeAl_2O_4$). Phys Chem Minerals 14:426-434

Hazen RM (1993) Comparative compressibilities of silicate spinels: anomalous behavior of $(Mg,Fe)_2SiO_4$. Science 259:206-209

Hazen RM, Downs RT, Finger LW (1996) High-pressure crystal chemistry of $LiScSiO_4$: An olivine with nearly isotropic compression. Am Mineral 81:327-334

Hazen RM, Weinberger MB, Yang H, Prewitt CT (2000) Comparative high-pressure crystal chemistry of wadsleyite, γ-$(Mg_{1-x}Fe_x)_2SiO_4$, with $x = 0$ and 0.25. Am Mineral 85:770-777

Hill FC, Gibbs GV, Boisen MB Jr. (1994) Bond stretching force constants and compressibilities of nitride, oxide, and sulfide coordination polyhedra in molecules and crystals. Structural Chem 6:349-355

Hochella MF, Brown GE, Ross FK, Gibbs GV (1979) High-temperature crystal chemistry of hydrous Mg-Fe-cordierites. Am Mineral 64:337-351

Hugh-Jones DA, Angel RJ (1994) A compressional study of $MgSiO_3$ orthoenstatite up to 8.5 GPa. Am Mineral 79:405-410

Hugh-Jones DA, Chopelas A, Angel RJ (1997) Tetrahedral compression in $(Mg,Fe)SiO_3$ orthopyroxenes. Phys Chem Minerals 24:301-310

Karplus M, Porter RN (1970) Atoms and Molecules: An Introduction for Students of Physical Chemistry. W.A. Benjamin, Menlo Park, California

Kudoh Y, Takeda H (1986) Single-crystal X-ray diffraction study on the bond compressibility of fayalite, Fe_2SiO_4, rutile, TiO_2, under high pressure. Physica 139 & 140B:333-336

Lager GA, Meagher EP (1978) High-temperature structural study of six olivines. Am Mineral 63:365-377

Levien L, Prewitt CT (1981) High-pressure structural study of diopside. Am Mineral 66:315-323

Mao H-k, Hemley RJ (1998) New windows on the Earth's deep interior. *In* Ultrahigh-Pressure Mineralogy: Physics and Chemistry of the Earth's Deep Interior. Hemley RJ (ed), Rev Mineral 37:1-32

Mary TA, Evans JSO, Vogt T, Sleight AW (1996) Negative thermal expansion from 0.3 to 1050 Kelvin in ZrW_2O_8. Science 272:90-92

Miletich R, Reifler H, Kunz M (1999) The "ETH diamond-anvil cell" design for single-crystal XRD at non-ambient PT conditions. Acta Crystallogr A55 Supplement: Abstr P08.CC.001

O'Keeffe M, Hyde BG (1981) Nonbonded forces in crystals. *In* Structure and Bonding in Crystals. O'Keeffe M, Navrotsky A (eds). Academic Press, New York, p 227-254

Ohashi Y (1982) A program to calculate the strain tensor from two sets of unit-cell parameters. *In* Hazen RM and Finger LW, Comapartive Crystal Chemistry. Wiley, New York, p 92-102

Ohashi Y, Burnham CW (1973) Clinopyroxene lattice deformations: The roles of chemical substitution and temperature. Am Mineral 58:843-849

Ohashi Y, Finger LW (1973) Lattice deformation in feldspars. Carnegie Inst Washington Year Book 72:569-573

Pasternak MP, Rozenberg GK, Machavariani GY, Naaman O, Taylor RD, Jeanloz R (1999) Breakdown of the Mott-Hubbard state in Fe_2O_3: A first-order insulator-metal transition with collapse of magnetism at 50 GPa. Phys Rev Lett 82:4663-4666

Pauling L (1960) The Nature of the Chemical Bond and the Structure of Molecules and Crystals: An Introduction to Modern Structural Chemistry, 3rd Edn. Cornell University Press, Ithaca, New York

Prewitt CT (1977) Effect of pressure on ionic radii (abstr). Geol Soc Am Abstr with Programs 9:1134

Rao KVK (1974) Thermal expansion and crystal structure. Am Inst Physics Conf Proc 17:219-230

Robinson K, Gibbs GV, Ribbe PH (1971) Quadratic elongation: a quantitative measure of distortion in coordination polyhedra. Science 172:567-570

Roy R, Agrawal D, McKinstry HA (1989) Very low thermal expansion coefficient materials. Ann Rev Mater Sci 19:59-81

Shannon RD, Prewitt CT (1970) Revised values of effective ionic radii. Acta Crystallogr B26:1046-1048

Shannon RD (1976) Revised effective ionic radii and systematic studies of interatomic distances in halides and chalcogenides. Acta Crystallogr A32:751-767

Sharp ZD, Hazen RM, Finger LW (1987) High-pressure crystal chemistry of monticellite $CaMgSiO_4$. Am Mineral 72:748-755

Shomaker V, Trueblood KN (1968) On the rigid-body motion of molecules in crystals. Acta Crystallogr B24:63-76

Slater JC (1963) Quantum Theory of Molecules and Solids. McGraw-Hill, New York

Staun Olsen J, Cousins CSG, Gerward L, Jhans H, Sheldon BJ (1991) A study of the crystal structure of Fe_2O_3 in the pressure range up to 65 GPa using synchrotron radiation. Physica Scripta 43:327-330

Sueno S, Cameron M, Papike JJ, Prewitt CT (1973) The high-temperature crystal chemistry of tremolite. Am Mineral 61:38-53

Swanson DK, Peterson RC (1980) Polyhedral volume calculations. Can Mineral 18:153-156

Takeda H, Morosin B (1975) Comparison of observed and predicted structural parameters of mica at high temperatures. Acta Crystallogr B31:2444-2452

Thompson RM, Downs RT (1999) Quantitative analysis of the closest-packing of anions in mineral structures as a function of pressure, temperature, and composition [abstr]. Trans Am Geophys Union Eos 80:F1107

Thompson RM, Downs RT (2001) Quantifying distortion from ideal closest-packing in a crystal structure with analysis and application. Acta Crystallographica B (in press)

Waser J, Pauling L (1950) Compressibilities, force constants, and interatomic distances of the elements in the solid state. J Chem Phys 18:747-753

Wechsler BA, Prewitt CT (1984) Crystal structure of ilmenite at high temperature and high pressure. Am Mineral 69:176-185

White GK (1973) Thermal expansion of reference materials: copper, silica and silicon. J Physics D6: 2070-2076

Winter JK, Ghose S, Okamura FP (1977) A high-temperature study of the thermal expansion and the anisotropy of the sodium atom in low albite. Am Mineral 62:921-931

Yang H, Hazen RM, Finger LW, Prewitt CT, Downs RT (1997a) Compressibility and crystal structure of sillimanite, Al_2SiO_5, at high pressure. Phys Chem Minerals 25:39-47

Yang H, Downs RT, Hazen RM, Prewitt CT (1997b) Compressibility and crystal structure of kyanite, Al_2SiO_5, at high pressure. Am Mineral 82:467-474

Yang H, Hazen RM (1999) Comparative high-pressure crystal chemistry of karrooite, $MgTi_2O_5$, with different ordering states. Am Mineral 84:130-137

Zhang L, Ahsbahs H, Hafner SS, Kutoglu A (1997) Single-crystal compression and crystal structure of clinopyroxene up to 10 GPa. Am Mineral 82:245-258

Zhang L, Ahsbahs H, Kutoglu A (1998) Hydrostatic compression and crystal structure of pyrope to 33 GPa. Phys Chem Minerals 19:507-509

Zuo JM, Kim M, O'Keeffe M, Spence JCH (1999) Direct observation of d-orbital holes and Cu-Cu bonding in Cu_2O. Nature 401:49-52